Journal of Sound and Vibration (2003) **259**(3), 625–636
doi:10.1006/jsvi.2002.5096, available online at http://www.idealibrary.com on IDEAL®

INSERTION LOSS OF A CAVITY-BACKED SEMI-CYLINDRICAL ENCLOSURE PANEL

Y. Y. Lee

Department of Building and Construction, City University of Hong Kong, 83 *Tat Chee Avenue Kowloon Tong, Kowloon, Hong Kong, People's Republic of China. E-mail: bcraylee@cityu.edu.hk*

(*Received* 14 *January* 2002)

In this paper, the insertion loss of a cavity-backed semi-cylindrical enclosure panel is studied theoretically and experimentally. The classical approach based on Narayanan [1] and Lee [2] is employed to the semi-cylindrical enclosure modelling. The theoretical model considers the three-dimensional acoustic modes of the semi-cylindrical cavity and the noise source vibration mode shape. The experimental result agrees reasonably with the theoretical prediction. It is found that the higher structural resonance in the semi-cylindrical can significantly deteriorate the insertion loss performance while only the (1,1) mode structural resonance in the rectangular models is the important one. The noise source panel vibrating in the (3,1) mode shape induces higher air pressure on the semi-cylindrical panel through the air cavity than the (1,1) mode shape.

1. INTRODUCTION

In the past, many researchers such as Narayanan [1], Lee [2–7], Lyon [8], Pretlove [9], Jackson [10], Guy [11], Dowell [12] and Oldham [13, 14] developed their models to predict the insertion loss performance or transmission loss performance of a cavity-backed rectangular enclosure panel. Their predictions have clearly indicated that the (1,1) mode structural resonance is much more important than others on the noise reduction performance

Although the rectangular enclosure models [1–14] and the present enclosure model are simplified and different from a practical close-fitting enclosure which has more than one panel and boundary conditions are more complicated, the theoretical predictions provide a close look at the importance of the acoustical and structural resonance. In many practical cases, it has been found that the measured insertion loss is lower than the predicted insertion loss which is calculated by conventional formulas. This phenomenon provides evidence to show that the acoustical resonance, higher order structural resonance, and noise source vibration mode shape play important roles in insertion loss prediction.

In references [1–13], the authors adopted the classical plate theory, and the series solution approach or Fourier transform technique for solving the equation of motion of the enclosure panel and the sound wave differential equation of the rectangular cavity respectively. In this paper, the theoretical approach based on references [1, 2] is employed to the entire semi-cylindrical enclosure modelling. The study of insertion loss of a cavity-backed semi-cylindrical enclosure panel is presented. The effects of noise source vibration mode shape, enclosure panel dimension, acoustic resonance and structural resonance on

0022-460X/02/$35.00

the insertion loss, are studied. The comparison between numerical and experimental results shows the validity of the theoretical model.

2. ACOUSTIC VELOCITY POTENTIAL

The semi-cylindrical enclosure model to be considered is shown in Figure 1 and consists of an acoustically hardwalled at $z = 0$ and L. The other two flexible vibrating plates are at ($\theta = 0$ and π, $r = R$). The vibrating flat panel is used as a noise source while the semi-cylindrical panel is used to reduce the noise induced. The acoustic velocity potential inside the semi-cylindrical cavity is given by the following wave equation:

$$\nabla^2 \Omega - \frac{1}{C_a^2}\frac{\partial^2 \Omega}{\partial t^2} = 0, \tag{1}$$

where the operator "∇" is in the cylindical form, i.e., $\vec{r}\partial/\partial r + \vec{\theta}\partial/r\partial\theta + \vec{z}\partial/\partial z$ and C_a is the sound speed.

The vibration velocities in the radial, tangential, and longitudinal directions and pressures within the air cavity can be derived from following equations:

$$\dot{r} = \frac{\partial \Omega}{\partial r}, \quad \dot{\theta} = \frac{\partial \Omega}{r\partial\theta}, \quad \dot{z} = \frac{\partial \Omega}{\partial z}, \quad P = -\rho_a \frac{\partial \Omega}{\partial t}, \tag{2a, b, c, d}$$

where ρ_a is the air density.

Here, r, θ, and Z are taken to be the radial, tangential and longitudinal displacements of air cavity at corresponding co-ordinates, so that their velocities are marked with dot sign. It is assumed that (P, Q) is the dominant mode of the semi-cylindrical panel, the flat source panel is forced to vibrate in (S, T) mode shape with constant velocity. P and S are odd numbers. Then the boundary conditions of the semi-cylindrical model to be satisfied are:

$$\dot{r} = \left.\frac{\partial \Omega}{\partial r}\right|_{r=R} = w_{cy}^{PQ} \mathrm{i}\omega\, \mathrm{e}^{\mathrm{i}\omega t} \sin(P\theta) \sin\left(\frac{Q\pi}{L} z\right), \tag{3a}$$

$$r\dot{\theta} = \left.\frac{\partial \Omega}{\partial \theta}\right|_{\theta=0} = w_{sou}^{ST} \mathrm{i}\omega\, \mathrm{e}^{\mathrm{i}\omega t} \cos\left(\frac{S\pi}{2R} r\right) \sin\left(\frac{T\pi}{L} z\right), \tag{3b}$$

$$r\dot{\theta} = \left.\frac{\partial \Omega}{\partial \theta}\right|_{\theta=\pi} = -w_{sou}^{ST} \mathrm{i}\omega\, \mathrm{e}^{\mathrm{i}\omega t} \cos\left(\frac{S\pi}{2R} r\right) \sin\left(\frac{T\pi}{L} z\right), \qquad \dot{z} = \left.\frac{\partial \Omega}{\partial z}\right|_{z=0,L} = 0, \tag{3c, d}$$

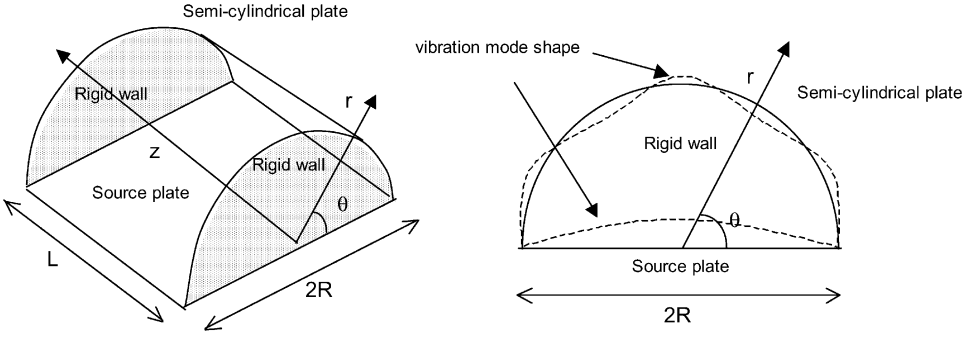

Figure 1. Semi-cylindrical enclosure model.

where w_{cy}^{PQ} is the (P, Q) modal displacement amplitude of the semi-cylindrical panel, w_{sou}^{ST} the (S, T) modal displacement amplitude of the source panel and i is the complex number $\sqrt{-1}$.

The solution of the above wave equation can be solved by transformation of homogeneous differential equation with non-homogeneous boundary conditions into a non-homogeneous differential equation with homogenous boundary conditions [15]. It can be regarded as $\Omega = \phi + \psi$ where ϕ is the general solution, and ψ is the particular solution. Now ψ is chosen to satisfy the boundary conditions in equations (3a–d) is shown below:

$$\psi = \sum_{W=0}\sum_{n=1} G^{nW}\, \mathrm{e}^{\mathrm{i}\omega t} \sin[(2n-1)\theta]\sin\left(\frac{n\pi r}{2R}\right)\cos\left(\frac{W\pi z}{L}\right) + \sum_{W=0}\sum_{N=1} K^{NW}\, \mathrm{e}^{\mathrm{i}\omega t}\cos(N\theta)\sin\left(\frac{\pi r}{R}\right)\cos\left(\frac{W\pi z}{L}\right), \tag{4}$$

where n and N are the numbers of circumferential waves for the particular solution ψ, W the number of axial half-waves, and G^{nW} and K^{NW} are the coefficients to be determined.

By using the boundary conditions in equations (3a–c), the two coefficients G_{nW} and K_{NW} can be determined. Substituting ψ into the boundary conditions $\theta = 0$ and π, gives

$$\left.\frac{1}{r}\frac{\partial\psi}{\partial\theta}\right|_{\theta=0 \text{ or } \theta=\pi} = \sum_{W=0}\sum_{n=1} G^{nW}\mathrm{e}^{\mathrm{i}\omega t}(2n-1)\frac{\sin((n\pi/2R)r)}{r}\cos\left(\frac{W\pi}{L}z\right) = \mathrm{i}\omega w_{sou}^{ST}\mathrm{e}^{\mathrm{i}\omega t}\cos\left(\frac{S\pi}{2R}r\right)\sin\left(\frac{T\pi}{L}z\right). \tag{5}$$

By multiplying cosine and sine on both sides and integrating across the panel surface, G_{nW} can be found by

$$G^{nW} = w_{sou}^{ST} g_{sou}, \tag{6}$$

where

$$g_{sou} = \frac{1}{R/2\, L/2}\frac{\mathrm{i}\omega}{(2n-1)}\int_0^L\int_0^R r\cos\left(\frac{S\pi}{2R}r\right)\sin\left(\frac{n\pi}{2R}r\right)\mathrm{d}r\sin\left(\frac{T\pi}{L}z\right)\cos\left(\frac{W\pi}{L}z\right)\mathrm{d}z.$$

Similarly, substituting ψ into the boundary condition $r = R$ gives

$$\left.\frac{\partial\psi}{\partial r}\right|_{r=R} = \sum_{W=0}\sum_{n=1} G^{nW}\,\mathrm{e}^{\mathrm{i}\omega t}\sin((2n-1)\theta)\left(\frac{n\pi}{2R}\cos\left(\frac{n\pi}{2}\right)\right)\cos\left(\frac{W\pi}{L}z\right) - \sum_{W=0}\sum_{N=1} K^{NW}\,\mathrm{e}^{\mathrm{i}\omega t}\cos(N\theta)\frac{\pi}{R}\cos\left(\frac{W\pi}{L}z\right) = \mathrm{i}\omega\mathrm{e}^{\mathrm{i}\omega t} w_{cy}^{PQ}\sin(P\theta)\sin\left(\frac{Q\pi z}{L}\right). \tag{7}$$

By using the orthogonal property of sine and cosine again and substituting equation (6) into equation (7), K^{NW} can be found by

$$K^{NW} = w_{sou}^{ST} k_{sou} + w_{cy}^{PQ} k_{cy}, \tag{8}$$

where

$$k_{sou} = \sum_{n=1} \frac{\mathrm{i}\omega g_{sou}((n\pi/2R)\cos(n\pi/2))}{(\pi/R)(\pi/2)(L/2)} \int_0^L \int_0^\pi \sin((2n-1)\theta) \times \cos(N\theta)\,\mathrm{d}\theta \cos\left(\frac{W\pi}{L}z\right)\cos\left(\frac{W\pi}{L}z\right)\mathrm{d}z,$$

$$k_{cy} = -\frac{\mathrm{i}\omega}{(\pi/R)(\pi/2)(L/2)} \int_0^L \int_0^\pi \sin(P\theta)\cos(N\theta)\,\mathrm{d}\theta \sin\left(\frac{Q\pi}{L}z\right)\cos\left(\frac{W\pi}{L}z\right)\mathrm{d}z.$$

Then the wave equation is expressed as a series of standard cylindrical separable functions, $\cos(U\theta)Ju(\beta^{UV}r)\cos(W\pi z/L)$. Let F^{UVW} is the modal coefficients,

$$\sum_{U=0}\sum_{V=0}\sum_{W=0} F^{UVW}\mathrm{e}^{\mathrm{i}\omega t}\cos(U\theta)\mathrm{J}u(\beta^{UV}r)\cos\left(\frac{W\pi}{L}z\right) = -\nabla^2\psi + \frac{1}{C_a^2}\frac{\partial^2\psi}{\partial t^2}, \tag{9}$$

where $\mathrm{J}u(\beta^{uv}r)$ is the Bessel function, $\mathrm{J}u'(\beta^{uv}R) = 0$, U the number of circumferential waves for the general solution ϕ, and V is the counting number for the sequence U of zeros of $\mathrm{J}u'(\beta^{uv}R) = 0$.

Due to the orthogonality of Bessel function and cosine function, F^{UVW} can be found by multiplying both sides of equation (10) with $r\cos(U\theta)\mathrm{J}u(\beta^{UV}r)$ and integrating across the enclosed volume:

$$F^{UVW} = \frac{\int_0^L\int_0^R\int_0^\pi \left(-\nabla^2\psi + \frac{1}{C_a^2}\frac{\partial^2\psi}{\partial t^2}\right)\cos(U\theta)\mathrm{J}u(\beta^{UV}r)\cos\left(\frac{W\pi}{L}z\right)\mathrm{d}\theta\,\mathrm{d}r\,\mathrm{d}z}{\mathrm{e}^{\mathrm{i}\omega t}\int_0^L\int_0^R\int_0^\pi \cos^2(U\theta)r\mathrm{J}u(\beta^{UV}r)^2\cos\left(\frac{W\pi}{L}z\right)\mathrm{d}\theta\,\mathrm{d}r\,\mathrm{d}z}. \tag{10}$$

It is necessary to express F^{UVW} in terms of the modal amplitudes of the source plate and the cylindrical plate. Let f_{sou} and f_{cy} are the modal coefficients which precede the terms of the modal amplitudes. Then,

$$F^{UVW} = (w_{sou}^{ST} f_{sou} + w_{cy}^{PQ} f_{cy}), \tag{11}$$

where

$$f_{sou} = \sum_{n=1} g_{sou}\, fg_{sou} + k_{sou}\, fk_{sou}, \quad f_{cy} = k_{cy}\, fk_{cy}, \quad fk_{sou} = fk_{cy},$$

$$fg_{sou} = \frac{1}{\int_0^\pi\int_0^R \mathrm{J}u(\beta^{UV}r)^2 r\cos^2(U\theta)\,\mathrm{d}r\,\mathrm{d}\theta}\left\{fg1\left[-\left(\frac{\omega}{C_a}\right)^2 + \left(\frac{\pi W}{L}\right)^2 + \left(\frac{n\pi}{2R}\right)^2\right] - fg2\left(\frac{n\pi}{2R}\right) + fg3(2n-1)^2\right\},$$

$$fk_{cy} = \frac{1}{\int_0^\pi\int_0^R \mathrm{J}u(\beta^{UV}r)^2 r\cos^2(U\theta)\,\mathrm{d}r\,\mathrm{d}\theta}\left\{fk1\left[-\left(\frac{\omega}{C_a}\right)^2 + \left(\frac{\pi W}{L}\right)^2 + \left(\frac{\pi}{R}\right)^2\right] - fk2\left(\frac{\pi}{R}\right) + fk3_{UV}U^2\right\},$$

$$fg1 = \int_0^\pi\int_0^R r\sin\left(\frac{n\pi}{2R}r\right)\mathrm{J}u(\beta^{UV}r)\sin((2n-1)\theta)\cos(U\theta)\mathrm{d}r\,\mathrm{d}\theta,$$

$$fk1 = \int_0^\pi\int_0^R r\sin\left(\frac{\pi}{R}r\right)\mathrm{J}u(\beta^{UV}r)\cos^2(U\theta)\mathrm{d}r\,\mathrm{d}\theta,$$

$$fg2 = \int_0^{\pi}\int_0^{R} \cos\left(\frac{n\pi}{2R}r\right) \mathrm{J}u(\beta^{UV}r)\sin((2n-1)\theta)\cos(U\theta)\mathrm{d}r\,\mathrm{d}\theta,$$
$$fk2 = \int_0^{\pi}\int_0^{R} \cos\left(\frac{\pi}{R}r\right) \mathrm{J}u(\beta^{UV}r)\cos^2(U\theta)\mathrm{d}r\,\mathrm{d}\theta,$$

$$fg3 = \int_0^{\pi}\int_0^{R} \frac{\sin((n\pi/2R)r)}{r} \mathrm{J}u(\beta^{UV}r)\sin((2n-1)\theta)\cos(U\theta)\mathrm{d}r\,\mathrm{d}\theta,$$
$$fk3 = \int_0^{\pi}\int_0^{R} \frac{\sin((\pi/R)r)}{r} \mathrm{J}u(\beta^{UV}r)\cos^2(U\theta)\mathrm{d}r\,\mathrm{d}\theta.$$

The general solution ϕ must satisfy the homogenous boundary conditions:

$$\dot{r} = \left.\frac{\partial\phi}{\partial r}\right|_{r=R} = 0, \quad r\dot{\theta} = \left.\frac{\partial\phi}{r\partial\theta}\right|_{\theta=0} = 0, \quad \dot{z} = \left.\frac{\partial\phi}{\partial z}\right|_{z=0 \text{ or } z=L} = 0. \qquad (12a-c)$$

Then, ϕ is chosen and given by

$$\phi = \sum_{U=0}\sum_{V=0}\sum_{W=0} B^{UVW}\cos(U\theta)\mathrm{J}u(\beta^{UV}r)\cos\left(\frac{W\pi z}{L}\right)\mathrm{e}^{\mathrm{i}\omega t}, \qquad (13)$$

where B^{UVW} is the coefficient to be determined.

By substituting $\Omega = \phi + \psi$ into equation (1). It gives

$$\nabla^2\phi - \frac{1}{C_a^2}\frac{\partial^2\phi}{\partial t^2} = -\nabla^2\psi + \frac{1}{C_a^2}\frac{\partial^2\psi}{\partial t^2}. \qquad (14)$$

Finally, by substituting equations (9) and (13) into equation (14), B^{UVW} can be found by

$$\nabla^2\phi - \frac{1}{C_a^2}\frac{\partial^2\phi}{\partial t^2} = \sum_{U}^{\infty}\sum_{V}^{\infty}\sum_{W}^{\infty} F_{UVW}\cos(U\theta)\mathrm{J}u(\beta_{UV}r)\cos\left(\frac{W\pi}{L}z\right)\mathrm{e}^{\mathrm{i}\omega t}$$
$$\Rightarrow \sum_{U=0}\sum_{V=0}\left(\frac{\omega^2-\omega_{UVW}^2}{C_a^2}\right)B^{UVW}\cos(U\theta)\mathrm{J}u(\beta^{UV}r)\mathrm{e}^{\mathrm{i}\omega t} = \sum_{U=0}\sum_{V=0} F^{UVW}\cos(U\theta)\mathrm{J}u(\beta^{UV}r)\mathrm{e}^{\mathrm{i}\omega t}$$
$$\Rightarrow B^{UVW} = \frac{C_a^2}{\omega^2-\omega_{UVW}^2}F^{UVW}$$
$$\Rightarrow B^{UVW} = \mathrm{i}w_{sou}^{ST}\times B_{sou}^{UVW} + \mathrm{i}w_{cy}^{PQ}\times B_{cy}^{UVW}, \qquad (15)$$

where

$$\omega_{UVW} = C_a\sqrt{\left(\frac{W\pi}{L}\right)^2 + (\beta^{UW})^2}, \qquad B_{sou}^{UVW} = \frac{-\mathrm{i}C_a^2}{\omega^2-\omega_{UVW}^2}f_{sou},$$

$$B_{cy}^{UVW} = \frac{-\mathrm{i}C_a^2}{\omega^2-\omega_{UVW}^2}f_{cy}.$$

To include the effect of acoustic damping, one may introduce a complex term, $2\eta_{UVW}\omega_{UVW}\omega\mathrm{i}$ (where η_{UVW} is the acoustic damping ratio of the (U, V, W) mode),

B_{sou}^{UVW} and B_{cy}^{UVW} can be rewritten as

$$B_{sou}^{UVW} = \frac{-\mathrm{i}C_a^2}{\omega^2 + 2\eta_{UVW}\omega_{UVW}\omega\mathrm{i} - \omega_{UVW}^2} f_{sou}, \tag{16a}$$

$$B_{cy}^{UVW} = \frac{-\mathrm{i}C_a^2}{\omega^2 + 2\eta_{UVW}\omega_{UVW}\omega\mathrm{i} - \omega_{UVW}^2} f_{cy}. \tag{16b}$$

3. STRUCTURAL VIBRATION

Consider the air pressure at the face $r = R$, which is induced by the constant vibration motion of the source panel. The natural frequencies of a semi-cylindrical plate, which four edges are simply supported, can be calculated by the following equation [16]:

$$\omega_{PQ} = \left(\frac{Eh^2}{12(1-v^2)\rho'} \left(\left(\frac{P\pi}{a}\right)^2 + \left(\frac{Q\pi}{L}\right)^2 \right)^2 + \frac{E}{(1-v^2)\rho' R^2} \frac{\left(\frac{Q\pi}{L}\right)^4}{\left(\left(\frac{P\pi}{a}\right)^2 + \left(\frac{Q\pi}{L}\right)^2 \right)^2} - \frac{Eh^2}{12(1-v^2)\rho' R^4} \frac{\left(\frac{P\pi R}{a}\right)^2 (4-v) - 2 - v}{2(1-v} \right)^{1/2}, \tag{17}$$

where ω_{PQ} is the natural frequency, E is Young's modulus, v the Poisson ratio, h the panel thickness, ρ' the panel density, L the longitudinal length, a the circumferential length $= \pi R$ and R is the radius of semi-cylindrical panel.

Consider the modal forced and damped motion of the semi-cylindrical panel due to air pressure force at $r = R$,

$$-\rho' h\omega^2 w_{cy}^{PQ} - 2\rho' h\xi_{PQ}\omega_{PQ}\omega w_{cy}^{PQ} i + D^{PQ} w_{cy}^{PQ} = -P_R^{PQ}, \tag{18}$$

where D^{PQ} is the (P, Q) mode rigidity $= \rho' h\omega_{PQ}^2$, ξ_{PQ} the (P, Q) mode structural damping ratio

$$P_R^{PQ} = \frac{\int_0^L \int_0^a P_R \sin(P\pi x/a)\sin(Q\pi z/L)\mathrm{d}x\,\mathrm{d}z}{(a/2)(L/2)} = \frac{\int_0^L \int_0^\pi P_R \sin(P\theta)\sin(Q\pi z/L)\mathrm{d}\theta\,\mathrm{d}z}{(\pi/2)(L/2)},$$

where $-P_R$ is the air pressure at $r = R$ and $x = R\theta$.

From equation (2d), the air pressure at $r = R$ can be found by

$$P_R = -\rho_a \mathrm{i}\omega \left[\sum_{U=0} \sum_{V=0} \sum_{W=0} B^{UVW} \mathrm{e}^{\mathrm{i}\omega t} \mathrm{J}u(\beta^{UV} R)\cos(U\theta)\cos\left(\frac{W\pi z}{L}\right) \times \sum_{n=1} \sum_{W=0} G^{nW}\, \mathrm{e}^{\mathrm{i}\omega t} \sin(2n-1)\theta \sin\left(\frac{n\pi}{2}\right)\cos\left(\frac{W\pi z}{L}\right) \right]. \tag{19}$$

Substituting equation (19) into equation (18), we can find out the ratio of the source panel and the semi-cylindrical panel vibrating amplitudes,

$$\frac{w_{cy}^{PQ}}{w_{sou}^{ST}} = \frac{\sum_{U=0}\sum_{V=0}\sum_{W=0} \alpha_{PQ}^{UW} B_{sou}^{UVW} \mathrm{J}u(\beta^{UV} R) + \sum_{W=0}\sum_{n=0} \kappa_{PQ}^{nW} G^{nW}}{[\rho' h(-\omega^2 - 2\rho' h\xi_{PQ}\omega_{PQ}\omega + \omega_{PQ}^2)] + \rho_a \omega \sum_{U=0}\sum_{V=0}\sum_{W=0} \alpha_{PQ}^{UW} B_{cy}^{UVW} \mathrm{J}u(\beta^{UV} R)}, \tag{20}$$

where

$$\alpha_{PQ}^{UW} = \frac{\int_0^L \int_0^\pi \cos(U\theta)\cos((W\pi/L)z)\sin(P\theta)\sin((Q\pi/L)z)\,\mathrm{d}\theta\,\mathrm{d}z}{(\pi/2)(L/2)},$$

$$\kappa_{PQ}^{nW} = \frac{\int_0^L \int_0^\pi \sin((2n-1)\theta)\cos((W\pi/L)z)\sin(P\theta)\sin((Q\pi/L)z)\,\mathrm{d}\theta\,\mathrm{d}z}{(\pi/2)(L/2)}.$$

Using well-known Rayleigh's formula [17] for the relation between acoustic and vibration, we know that

$$SE = \sigma\, VE, \tag{21}$$

where SE is sound energy, VE is vibration energy, and σ is the radiation efficiency of the vibrating structure.

Using equations (20) and (21), the sound insertion loss is defined by

$$IL = -10\log\left(\frac{SE_{cy}}{SE_{sou}}\right) = -10\log\left(\left|\frac{w_{cy}^{PQ}}{w_{sou}^{ST}}\right|^2 \frac{A_{cy}\sigma_{cy}^{PQ}}{A_{sou}\sigma_{sou}^{ST}}\right), \tag{22}$$

where SE_{cy} and SE_{sou} are the sound energies radiated by the semi-cylindrical and source panels, respectively, A_{sou} and A_{cy} are the source and semi-cylindrical panel surface areas, σ_{sou}^{ST} is the radiation efficiency of the (S, T) mode of the source panel [3, 17], and σ_{cy}^{PQ} is the radiation efficiency of the (P, Q) mode of the semi-cylindrical panel [3, 18].

Consider the multi-mode response of the semi-cylindrical panel [7]. Equation (22) can be rewritten into a more general form as

$$IL = -10\log\left(\sum_{P=1}^{\bar{P}}\sum_{Q=1}^{\bar{Q}}\left|\frac{w_{cy}^{PQ}}{w_{sou}^{ST}}\right|^2 \frac{A_{cy}\sigma_{cy}^{PQ}}{A_{sou}\sigma_{sou}^{ST}}\right), \tag{23}$$

where $\bar{P}$ and $\bar{Q}$ are the structural mode numbers of the semi-cylindrical panel.

4. THEORETICAL RESULTS

In Figures 2(a–c), the theoretical insertion loss predictions for three semi-cylindrical panels with four simply supported boundaries which measure 20 cm in radius and 40 cm in length, 20 cm in radius and 120 cm in length, 60 cm in radius and 120 cm in length respectively. The material properties of the steel panel are as follows: Young's modulus $= 20 \times 10^{10}$ Pa, density $= 7800$ kg/m^3, the Poisson ratio $= 0{\cdot}3$, damping ratio $= 0{\cdot}02$. The (1,1), (3,1), (5,1) and (7,1) modes are used individually for representing the modal motions of the semi-cylindrical panel (thus equation (22) is used for the insertion loss prediction).

In the Figures 2(a–c), the source panel is assumed to vibrate only in the (1,1) mode. It should be noted that the (1,1) mode resonance of the semi-cylindrical panel in Figure 2(a) is outside the frequency range studied as the resonance frequency is about 3000 Hz. The (7,1) mode here has the lowest resonance frequency, 355 Hz. The second and the third lowest structural resonance frequencies are 408 Hz, (5,1) mode and 910 Hz, (3,1) mode respectively.

Among the three curves in Figure 2(a), the one representing the (3,1) mode curve gives lowest insertion loss values at the frequency range over 600 Hz. The most significant cavity resonance in the radial direction at 826 Hz superimposes on the structural resonance of the (3,1) mode. The interaction between the cavity resonance and structural resonance gives a

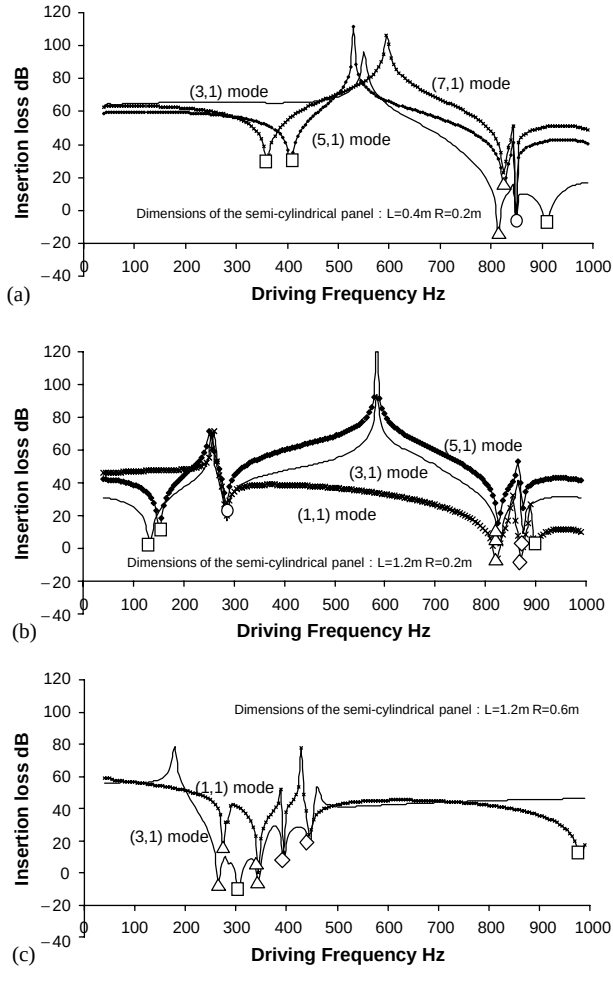

Figure 2. Different vibration mode shapes of the steel semi-cylindrical panel: source panel mode shape (1,1) mode. (a) length = 0·4 m, radius = 0·2 m; (b) length = 1·2 m, radius = 0·2 m; (c) length = 1·2 m, radius = 0·6 m. □, structural resonance; ○, cavity resonance in the longitudinal direction; △, cavity resonance in the radial; ◇ cavity resonance in the longitudinal and radial directions.

large and wide dip there. There is another dip around 850 Hz which is due to the cavity resonance in the longitudinal direction and affects over a very narrow frequency band.

In Figure 2(b), the (1,1) mode structural resonance and the fundamental cavity resonance in the radial direction strongly couple with each other to deteriorate the insertion loss at the frequency range 800–900 Hz. When compared with the dip due to the (1,1) mode structural resonance, the dips due to the (3,1) mode and the (5,1) mode weakly coupled with the acoustical resonance around 300 Hz are smaller. The curve representing the (3,1) mode generally gives lower insertion loss values than the (5,1) mode curve.

In Figure 2c, the (3,1) mode structural resonance and the fundamental cavity resonance strongly couple with each other to deteriorate the insertion loss at the frequency range 250–350 Hz. When compared with the dip due to the (3,1) mode structural resonance at about 300 Hz, the dip at about 960 Hz due to the (1,1) structural mode is much smaller.

Figure 3 shows the influence of the vibrating mode shape of the source panel on the insertion loss. It is assumed that the semi-cylindrical panel vibrates in the (3,1) mode shape

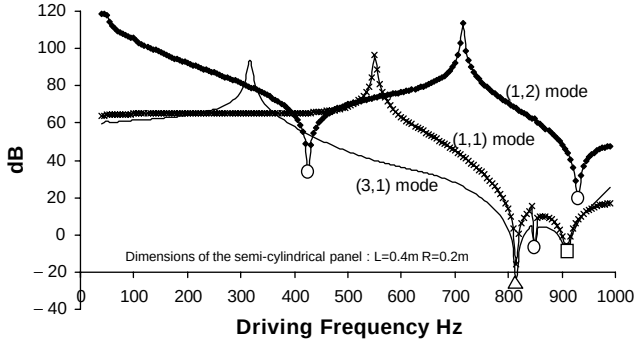

Figure 3. Different vibration mode shapes of the source panel: semi-cylindrical panel dimensions: length = 0·4 m, radius = 0·2 m. □, structural resonance; ○, cavity resonance in the longitudinal direction; △, cavity resonance in the radial direction.

when the source panel is vibrating in the (3,1) or (1,1) mode shape; the semi-cylindrical panel vibrates in the (3,2) mode shape when the source panel is vibrating in the (1,2) mode shape. In Figure 3, the (3,1) mode shape of the source panel of the semi-cylindrical enclosure model can result in lower insertion loss than the (1,1) mode shape. It can be seen that the dip of the (3,1) mode curve at frequencies 800–1000 Hz due to the structural resonance coupled with the acoustic resonance is wider and bigger than that of the (1,1) mode curve. This implies that the (3,1) mode shape of the source panel can induce higher air pressure on the semi-cylindrical panel through the air cavity. The (0,1) mode cavity resonance, which couples with antisymmetrical structural mode, makes another dip at about 420 Hz.

5. EXPERIMENTAL RESULTS

The measurement was carried out in the reverberant chamber in the Noise Laboratory of the Department of Civil and Structural Engineering of The Hong Kong Polytechnic University. In Figure 4, the model consists of a rectangular box constructed of 8 cm thick concrete walls and bottom, measuring 60 cm × 54 cm × 54 cm. The employed enclosure panel is a 1 mm steel semi-cylindrical plate measuring 42 cm in length and 19 cm in radius. The material properties of the steel panel are same as those in the theoretical cases. A rectangular box made of five 18 mm wooden panels and one 2 mm aluminum plate which was used as a source plate. The loudspeaker put into the wooden box and used for driving the aluminum source plate was 30 cm in diameter to simulate a noisy machine. The size of the loudspeaker was chosen as large as possible in order to give good performance at low frequencies. A wide band noise of 100–1000 Hz was generated from the loudspeaker. The sound power was measured by a sound level meter. The microphone positions lay on a hemispherical surface which enclosed the source and terminated on the reflecting plane. According to ISO 3746, the radius of the hemisphere should be at least twice the major source dimension. The average sound power over the hemisphere surface can be calculated by

$$L_w = \bar{L}_P + 10\log\frac{S_{hem}}{S_0} = 10\log_{10}\left[\frac{1}{N_{meas}}\sum_{i=1}^{N_{meas}} 10^{L_{Pi}/10}\right]\frac{S_{hem}}{S_0}, \tag{24}$$

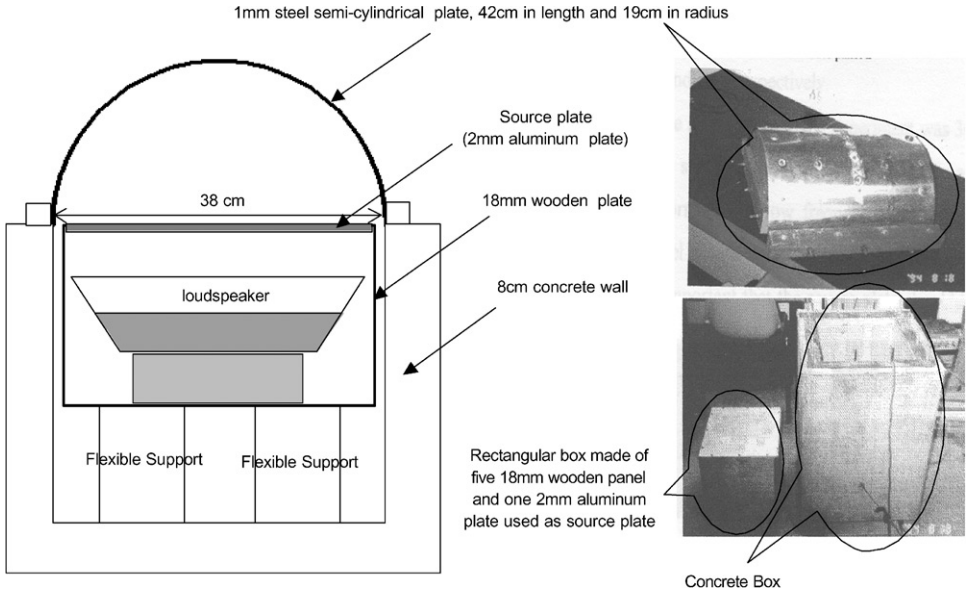

Figure 4. Experimental set-up.

where L_w is the sound power level, $\bar{L}_P$ the average sound pressure level, L_{Pi} the sound pressure level at ith measurement position, N_{mea} the total number of measurement positions, S_{hem} the surface area of hemisphere, $2\pi r^2$ and S_0 is the reference area $1\,\mathrm{m}^2$.

The loudspeaker could not keep the source plate vibrating with constant velocity amplitude. Consequently, for insertion loss measurement, error arouse due to "feedback loading" effect on the loudspeaker. The approach in reference [14] was employed to monitor the vibration amplitude of the source plate and to correct measured insertion loss for the feedback loading effect. The correction of the measured noise reduction for the "feedback loading" effect on the loudspeaker is given by

$$LC = 20 \log\left(\frac{A_u}{A_e}\right), \tag{25}$$

where LC is the loading correction, A_u the vibration amplitude of the unenclosed source panel and A_e the vibration amplitude of the enclosed source panel.

Then, the insertion loss can be calculated by

$$IL = L_u - L_e - LC, \tag{26}$$

where L_u is the sound power level of the unenclosed source panel and L_e is the sound power level of the enclosure panel.

The source plate was subject to a wide band acoustic pressure and vibrating in multi-modes over the frequency range 100–1000 Hz. Thus the insertion loss predictions of the (1,1), (1,3) and (2,1) modes of the source plate are used to compare with the experimental result in Figure 5. The solid line represents the prediction of the (1,1) mode; the solid line with squares represents the prediction of the (1,3) mode; and the solid line with rhomboids represents the prediction of the (2,1) mode. The boundary conditions are assumed simply supported in the theoretical prediction. Since the main uncertainty remains in the structural and acoustical damping loss factor, the prediction is somewhat different from the experimental result especially at the acoustic and structural resonant frequencies. At

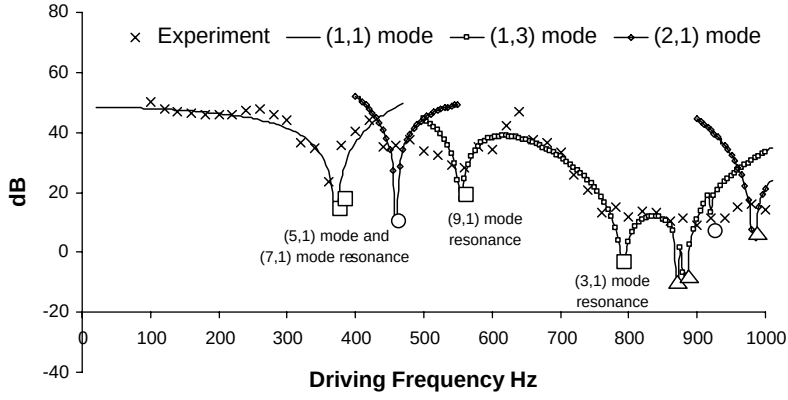

Figure 5. Experimental result and individual source mode predictions of the 1 mm steel semi-cylindrical panel: length = 0·42 m, radius = 0·19 m. □, structural resonance; ○, cavity resonance in the longitudinal direction; △, cavity resonance in the radial direction.

about 350 Hz, the vibrating mode shape of the semi-cylindrical panel is mainly the (5,1) mode shape and (7,1) mode shape (it is noted that the resonant frequencies of the (5,1) mode and (7,1) mode are 355 and 358 Hz respectively). Around this frequency, the source plate is mainly vibrating in the (1,1) mode and coupled with the (5,1) mode shape and (7,1) mode shape of the semi-cylindrical panel. At about 450 Hz, the acoustic resonance in the longitudinal direction (the (0,1) mode) occurs and couples with the antisymmetrical mode shapes of the semi-cylindrical panel and source plate (the (2,1) mode). At about 550 Hz, the vibrating mode shape of the semi-cylindrical panel is mainly the (9,1) mode shape (it is noted that the resonance frequency of the (9,1) mode is 550 Hz). At the frequency range, 800–900 Hz, the (3,1) mode structural resonance of the semi-cylindrical panel and the cavity resonance in the radial direction strongly couple with each other to deteriorate the insertion loss. Over the frequency range of 550–900 Hz, the source plate is manly vibrating in the higher mode (the (3,1) mode). At about 980 Hz, there is an acoustic resonance in the radial direction coupling with the antisymmetrical mode shapes of the semi-cylindrical panel and source plate (the (2,1) mode). It should be noted that the motions of the antisymmetrical mode shapes of the source plate cannot excite any symmetrical responses of the semi-cylindrical panel, which only couples with antisymmetrical mode shapes.

6. CONCLUSION

A model for predicting the insertion loss of a cavity-backed semi-cylindrical panel has been presented. The result of the measurements made to test the validity of the model suggests it can give a reasonable prediction. It is found that the structural resonance of the semi-cylindrical enclosure panel other than the (1,1) mode resonance in the semi-cylindrical model can significantly deteriorate the insertion loss performance. Also, the noise source panel vibrating in the (3,1) mode shape induces higher air pressure on the semi-cylindrical panel through the air cavity than the (1,1) mode.

ACKNOWLEDGMENTS

The research work was supported by the Strategic Research Grant (7001231-560) of City University of Hong Kong, Kowloon Tong, Kowloon, Hong Kong.

REFERENCES

1. S. Narayanan and R. L. Shanbhag, 1988 *Journal of Sound and Vibration* **150**, 251–270. Sound transmission through elastically supported sandwich panels into a rectangular enclosure.
2. Y. Y. Lee and C. F. Ng 1994 *The 5th International Conference on Recent Advances in Structural Dynamics, ISVR, U.K.,* July 1994, 1023–1032. The prediction of the effects of stiffness & damping on noise reduction of small enclosure.
3. Y. Y. Lee 1995 *M.Phil. Thesis, Deparment of Civil and Structural Engineering, The Hong Kong Polytechnic University*. Structural-acoustic analysis of close-fitting enclosures.
4. Y. Y. Lee and C. F. Ng 1995 *Proceedings of the International Conference on Structural Dynamics, Vibration, Noise and Control, Hong Kong,* December 1995, 1201–1206. The noise & vibration reduction of close fitting curved enclosure panels.
5. Y. Y. Lee and C. F. Ng 1997 *Journal of Building Acoustics* **2**, 549–567. The effects of coupled source/cavity modes on the acoustic insertion loss of close-fitting enclosures.
6. Y. Y. Lee and C. F. Ng 1997 *The 6th International Conference on Recent Advances in Structural Dynamics, ISVR, U.K.,* July 1997, 553–562, Insertion loss of stiffened enclosures.
7. Y. Y. Lee and C. F. Ng 1998 *Journal of Sound and Vibration* **217**, 239–260. Sound insertion loss of stiffened enclosure plates using the finite element method and the classical approach.
8. R. H. Lyon 1963 *Journal of the Acoustical Society of America* **35**, 1791–1797. Noise reduction of rectangular enclosures with one flexible wall.
9. A. J. Pretlove 1965 *Journal of Sound and Vibration* **2**, 197–209. Free vibrations of a rectangular backed by a closed rectangular cavity.
10. R. S. Jackson 1966 *Journal of Sound and Vibration.* **3**, 82–94. Some aspects of the performance acoustic hoods.
11. R. W. Guy 1973 *Journal of Sound Vibration* **27**, 207–223. The transmission of sound through a cavity-backed finite plate.
12. E. H. Dowell, G. F. Gorman and D. A. Smith 1977 *Journal of Sound and Vibration* **52**, 519–542. Acoustoelasticity: general theory, acoustical natural modes and forced response to sinusoidal excitation, including comparisons with experiment.
13. D. J. Oldham and S. N. Hillarby 1991 *Journal of Sound and Vibration* **150**, 261–281. The acoustical performance of small close fitting enclosures. Part 1 theoretical models.
14. D. J. Oldham and S. N. Hillarby 1991 *Journal of Sound and Vibration* **150**, 283–300. The acoustical performance of small close fitting enclosures, Part 2: experimental investigation.
15. H. F. Weinberger 1965 *A First Course in Partial Differential Equations.* New York: John Wiley & Sons.
16. L. Cremer and M. Heckl 1988 *Strucutre-Borne Sound.* Berlin Heidelberg: Springer-Verlag; second edition.
17. C. E. Wallace 1972 *Journal of the Acoustical Society of America* **51**, 946–952. Radiation resistance of a rectangular panel.
18. M. C. Jumger, and D. Feit 1986 *Sound Structures, and their Interaction*. Cambridge, MA: MIT Press.